Polymer 50 (2009) 1819–1829

Contents lists available at ScienceDirect

Polymer

journal homepage: www.elsevier.com/locate/polymer

Feature Article

Chain statistics in polyethylene crystallization

Giuseppe Allegra*, Antonino Famulari [1]

Politecnico di Milano, Dipartimento di Chimica, Materiali e Ingegneria Chimica "G. Natta", via Mancinelli 7, 20131 Milano, Italy

ARTICLE INFO

Article history:
Received 11 November 2008
Received in revised form
14 January 2009
Accepted 20 January 2009
Available online 7 February 2009

Keywords:
Polymer physics
Chain statistics
Polyethylene crystallization

ABSTRACT

The molecular mechanism of polyethylene crystallization in solution is revisited within the framework of the bundle model [Allegra G, Meille SV. Adv Polym Sci 2005;191:87]. Previous SANS/IANS results [Sadler DM, Keller A. Science 1979;203:263; Spells SJ, Sadler DM. Polymer 1984;25:739; Stamm M, Fischer EW, Dettenmaier M, Convert P. Faraday Disc Chem Soc 1979;68:263] from partially deuterated samples are used. It is proposed that the chain deposits on the growing lamella under the form of compact crystalline domains, their size being $\cong\sqrt{M_w}$. The radius of gyration of the crystallized chain agrees with a model consisting of a linear sequence of crystalline domains connected by chain segments with random orientations. It is suggested that the whole chain is in a bundle meta-stable equilibrium and collapses in the vicinity of the growing lamellar edge, then crystallizing around secondary nuclei. Compactness of the crystalline domains is correlated to prior chain collapse in the liquid state. The observed proportionality to $\sqrt{M_w}$ of the crystalline domain size is approximately explained.

1. Introduction

The molecular mechanism of polymer crystallization has been the subject of a considerable debate in the last decades. Whether from the melt, from solution or from the glass, under flux or under quiescent conditions, the issue of polymer crystallization has attracted much interest, both for its scientific and for its technological aspects [1–3]. An increasingly large body of experimental results [4–26] has been investigated through theoretical and simulation approaches, frequently complementing one another [10,11,27–53].

We shall concentrate on a few aspects inherent with quiescent crystallization of linear polyethylene from solution, that may be summarized by the question: What is the molecular mechanism of polyethylene crystallization in solution?

In the following, after reviewing concisely some relevant experimental information (Section 2), we provide elements to clarify that question. In Sections 3 and 4 we revisit the "bundle model" previously proposed by some of us [30–33], and in Section 5 we illustrate the molecular mechanism of crystallization from the bundle state of the chain. After a general discussion (Section 6) where structural proposals from other Authors are comparatively reviewed [2–9,19,22,23,35–39,48], concluding remarks follow (Section 7).

2. SANS/IANS diffraction data from solution-crystallized samples: model and structural considerations

The following results were obtained by two Groups of Authors, both of them by SANS–IANS neutron scattering on partially deuterated, un-fractionated polyethylene samples (M_w/M_n roughly around 2) with different molecular weights M_w. All the samples were crystallized at 60–70 °C from *o*-xylene solutions.

In Fig. 1 we show the "stacked-sheet" model proposed by Stamm, Fischer et al. and the corresponding comparison between experimental and calculated diffraction plot; the calculations were carried out by the same Authors [9]. In Fig. 2 we show a similar comparison of Kratky plots obtained by Spells and Sadler [7] from 4 samples with different molecular weights, with the diffraction spectra calculated by us (see Appendix A) from "stacked-sheet" models analogous to those of the previously quoted Authors [9]. Fig. 3 gives the SANS radius of gyration (R_g) from melt- and solution-crystallized, partially deuterated samples [4–8]; the solution results are dominated by the chain dimensions parallel to the plane of the lamellae [5]. The experimental results reported in Figs. 1–3 will represent the basis of our following analysis.

In Fig. 2, the stem arrangements (domains) shown in the right-hand side are to be regarded as averages; each chain is assumed to consist of spatially uncorrelated domains. Consistent with the observed fold length of about 100 Å for this undercooling degree

* Corresponding author. Tel.: +39 0223993023; fax: +39 0223993081.
E-mail addresses: giuseppe.allegra@polimi.it (G. Allegra), antonino.famulari@polimi.it (A. Famulari).
[1] Tel.: +39 0223993044; fax: +39 0223993081.

0032-3861/$ – see front matter © 2009 Elsevier Ltd. All rights reserved.
doi:10.1016/j.polymer.2009.01.063

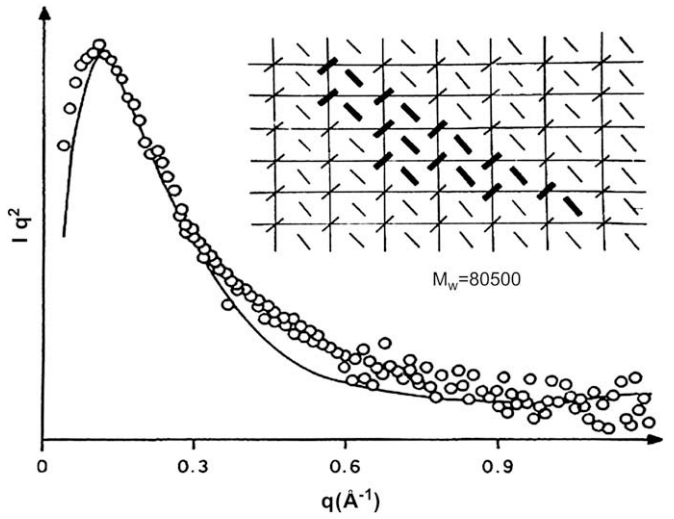

Fig. 1. Kratky plot from a partially deuterated polyethylene sample and corresponding structure of the crystalline domain, as seen parallel to the stem axis. The labelled chain is shown in heavy lines. (Taken from Ref. [9], authors Stamm, Fischer, Dettenmaier, Convert).

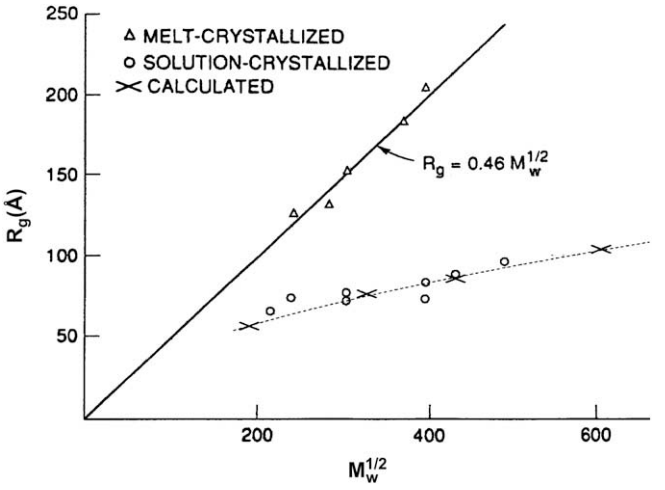

Fig. 3. SANS radius of gyration (R_g) from melt- and solution-crystallized, partially deuterated samples (solution data taken and reported by Sadler, Keller, Spells, see Refs. [4–8]). Note the difference between melt-crystallization (unperturbed chains) and solution crystallization (unperturbed chains).

($\Delta T = T_0 - T_C \sim 45\,^{\circ}C$, T_0 ideal melting temperature, T_C temperature of crystallization [31]), each stem is a rod-like sequence of (–CH_2–CH_2–) groups and is assumed to comprise about 80 C atoms; all the stems are placed at the same height with respect to a horizontal plane. The procedure to calculate the diffraction intensity is given in Appendix A.

As shown in Figs. 1 and 2, all the diffracting domains – henceforth (chain) crystalline domains – display a roughly similar shape, the ratio between their average thickness and width showing a modest increase with increasing overall size. Both the small distance from the chain axis of the diffracting H and D atoms and the small deviation from hexagonal symmetry of the stem axes in the orthorhombic unit cell, turn out to be essentially irrelevant on the diffraction results in the range $0 \le q\ (= ((2\pi \sin\theta)/(\lambda))) \le 0.25\ A^{-1}$. The average direction of elongation of the domains is parallel to the crystallographic direction (110) for orthorhombic PE [4]. We see that n_{stem} does not increase in a direct proportion with the molecular weight M_w. Fig. 4 shows a double-logarithmic plot of M_w vs. q_{max}, showing an approximate linear dependence, leading to the following power law:

$$(q_{max})^{-2} \propto n_{stem} \cong 0.22 \cdot M_w^{\alpha};\ \ \alpha = 0.50 \pm 0.03. \qquad (1)$$

Notice that the (approximate) shape similarity among the Kratky plots, suggesting analogous similarity among the crystalline chain domains is exploited, suggesting $(q_{max})^{-2} \propto n_{stem}$; we point out that $(q_{max})^{-2}$ has the dimensions of a surface and n_{stem} is proportional to the domain area projected along the stem axis. Eq. (1) may be summarized by

$$n_{stem} \approx \sqrt{M_w} \qquad (1')$$

It should be stressed that n_{stem} is an average for the particular M_w. Eq. (1) is independently validated by the following comparison among the calibrated peak intensities shown in Fig. 2. Let us first divide the Kratky peak intensity Iq^2_{peak} by Iq^2_{stem}, or the intensity diffracted by a single stem at the same q; we thus obtain the peak intensity diffracted from material points lying in a plane approximately orthogonal to the stem axes, each point replacing a whole stem. As shown theoretically by Guinier [20] and experimentally

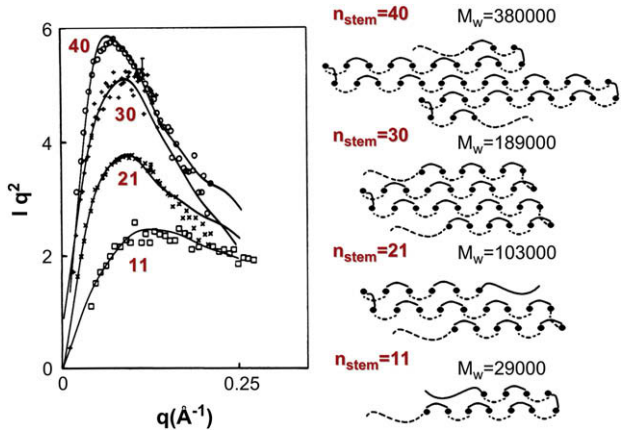

Fig. 2. Comparison between experimental Kratky plots reported by Spells and Sadler [7] from partially deuterated PE samples and the diffraction spectra calculated assuming the crystalline domain structures reported at right (see Appendix A for the calculations).

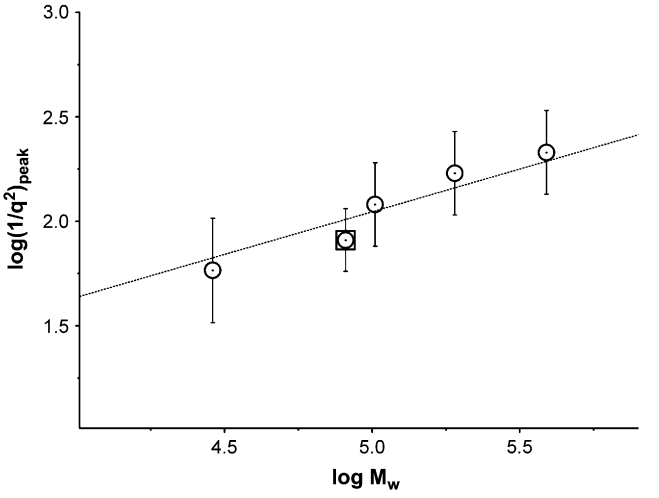

Fig. 4. Correlation between the q-coordinate at the peak of the Kratky plot, and M_w, from Figs. 1 and 2. The experimental point enclosed in a square is from Fig. 1 (Ref. [9]), the other points from Fig. 2 (Ref. [7]). Error bars are shown.

validated for isolated straight chains of deuterated dotriacontane $C_{32}D_{66}$ by Spells and Sadler (see Fig. 5 in Ref. [7]), Iq^2_{stem} is $\propto q$. Consequently we have

$$Iq^2_{\mathrm{reduced,\ peak}} = Iq^2_{\mathrm{peak}}/Iq^2_{\mathrm{stem}} \propto \left\{Iq^2/q\right\}_{\mathrm{peak}} = Iq_{\mathrm{peak}} \tag{2}$$

We show that the reduced intensity Iq_{peak} is expected to be proportional to the average stem numbers per crystalline domain n_{stem}. In fact, supposing at first that the whole sample reduces to a single crystalline domain, in the limit $q \to 0$ the diffraction amplitude should be proportional to n_{stem} and the diffracted intensity Iq_{peak} should be proportional to $(n_{\mathrm{stem}})^2$. Assuming a uniform crystallization degree for all the samples, with the same polymer mass in each sample, the number of chain crystalline domains – each of them having a polymer mass $\propto n_{\mathrm{stem}}$ – is $\propto 1/n_{\mathrm{stem}}$. Therefore the reduced intensity Iq_{peak} is $\propto (n_{\mathrm{stem}})^2 \times (1/n_{\mathrm{stem}}) = n_{\mathrm{stem}}$ for $q \to 0$. If the crystalline domains are large enough that the q-values at their peaks are sufficiently close to zero, this conclusion is approximately valid and we have $Iq_{\mathrm{peak}} \approx n_{\mathrm{stem}}$. This result appears to be validated by Fig. 5, where both the reduced peak intensities Iq_{peak} (from Fig. 2, on the ordinate) and the stem numbers n_{stem} (evaluated from the peak profiles of Fig. 2, on the abscissa) are the same as in Fig. 2. As it may be seen, Fig. 5 shows a substantial proportionality between Iq_{peak} and n_{stem}.

We point out that the diffracted intensities from the sample investigated by Stamm and co-workers [9] are not in the same scale as the data reported by Spells and Sadler [7], so that they cannot be used to fit into Fig. 5.

3. The chain model in the crystalline state: the radius of gyration

Experimental values of the radius of gyration (R_g) of crystallized chains were obtained by Sadler and Keller by SANS experiments [4–6]. Sedimented lamellar stacks were examined, the normal to the lamellae being approximately parallel to the beam direction. Therefore the results of R_g reported in Fig. 3 approximately correspond to the projection of the radius of gyration along the stem axis of the crystalline domains, all of them being parallel among themselves [6]; see Fig. 6 showing a sketchy model of the crystallized chain. The crystalline domains are assumed to be sequentially connected by chain segments, whose conformation is restricted by lamellar spatial constraints. Although with a small probability, crystalline domains of one chain might appear in different crystalline lamellae of the same lamellar stack [4–7].

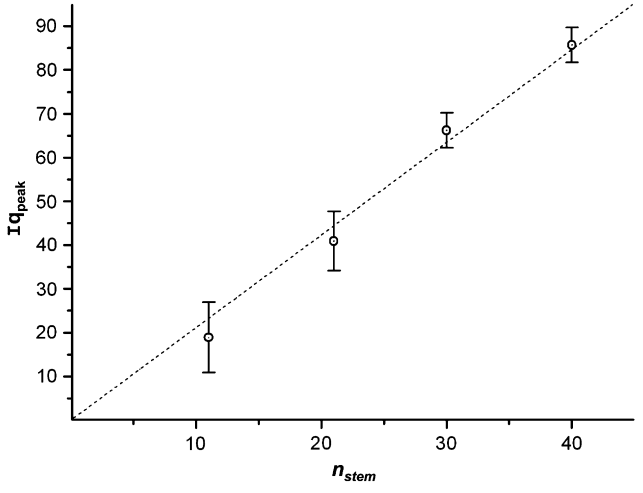

Fig. 5. Correlation between $Iq_{\mathrm{peak}} = Iq^2_{\mathrm{peak}}/q_{\mathrm{peak}}$ (see text) from the experimental data reported in Fig. 2. Error bars are shown.

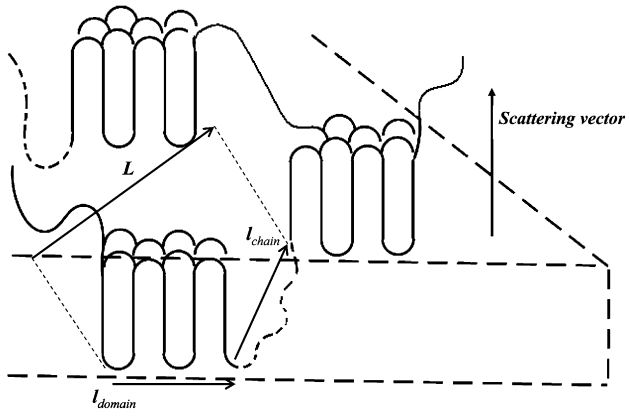

Fig. 6. Scheme showing crystalline domains produced by one chain inside a lamella and the characteristic average dimensions L, l_{domain}, l_{chain}, see text.

Denoting with n_c the number of (–CH_2–) units per crystalline stem, the mass of a crystalline domain is given by 14 $n_{\mathrm{stem}} \cdot n_c$ Da, and the average number of domains per chain is given by

$$\nu = \frac{M_w}{14 \cdot n_{\mathrm{stem}} \cdot n_c} \tag{3}$$

Although ν is not bound to be an integer, we shall formally regard it as such. As shown in Fig. 6, the connecting chain segments are supposed to be attached at opposite ends of the longer average dimension of each crystalline domain l_{domain}.

Neglecting end effects and considering the projection along the stem axis, see Fig. 6, for each of the ν domains we define a vector $\mathbf{L}$ that spans the domain itself plus the chain segment connecting with the following domain. For simplicity – and with no effective consequence on the calculated diffraction – in Fig. 6 we ignore the crystallographically ordered placement of the stems within the lamella. We see that $\mathbf{L}$ is $(\mathbf{l}_{\mathrm{domain}} + \mathbf{l}_{\mathrm{chain}})$, where $\mathbf{l}_{\mathrm{domain}}$ adjoins the two ends of the crystalline domain and $\mathbf{l}_{\mathrm{chain}}$ is the end-to-end vector of the connecting chain segment. Assuming absence of correlation between these vectors, we have

$$L^2 = l^2_{\mathrm{domain}} + l^2_{\mathrm{chain}};\ l^2_{\mathrm{domain}} = \langle \mathbf{l}^2_{\mathrm{domain}} \rangle;\quad l^2_{\mathrm{chain}} = \langle \mathbf{l}^2_{\mathrm{chain}} \rangle;\ L^2 = \left\langle \mathbf{L}^2 \right\rangle. \tag{4}$$

For two different crystalline domains we also assume $\langle \mathbf{L}_i \cdot \mathbf{L}_j \rangle = 0$, $i \neq j$. We end up with a freely jointed chain consisting of ν statistically equivalent units, or pseudo-atoms, connected with $(\nu - 1)$ uncorrelated pseudo-bonds; each unit has a mean-square length L^2. The root-mean-square radius of gyration R_g is given by [see Ref. [27], Ch1, Eq. (15), $\langle s^2 \rangle_0 \to R_g^2$, $n \to (\nu + 1)$]

$$R_g = \sqrt{R_g^2} = \sqrt{\frac{1}{6}\frac{\nu^2 - 1}{\nu} L^2} \tag{5}$$

As shown in Fig. 3 and Table 1, a reasonable fit with the experimental data is obtained by taking the (uniform) length of the connecting chain as $l_{\mathrm{chain}} = 82$ Å. Note that, regarding this chain as fully stretched, we have $82/1.27 = 65$ (–CH_2–) groups, i.e., a little less than one stem with 80 (–CH_2–) groups. If the connecting chain is regarded as unperturbed the number of (–CH_2–) groups is about 4 times larger. The relatively strong packing forces acting on the crystalline domains during lamellar crystallization may suggest

Table 1
Parameters to evaluate the plot of R_g vs. $M_w^{1/2}$, see Fig. 3. Distances are given in Å, $l_{chain} = 82$ Å and $n_c = 80$.

M_w	n_{stem}	$\nu = \frac{M_w}{14 \cdot n_{stem} \cdot n_c}$	l_{domain}	$L = \sqrt{l_{domain}^2 + l_{chain}^2}$	$R_g(\text{calc}) = L\sqrt{\frac{1}{6}\frac{\nu^2 - 1}{\nu}}$	R_g (obs)
29.000	11	2.35	26.0	86.0	48.7	<60
103.000	21	4.38	32.0	88.0	73.2	~75
189.000	30	5.63	34.0	88.8	84.7	~90
386.000	40	8.62	37.0	90.0	107.1	~100

that the connecting chains approach full extension. In any case, for our purposes the contribution of these chain segments to the observed diffraction should be negligible, as the main-peak diffraction region ($q < 0.25$ Å^{-1}, see Fig. 2) is dominated by interference effects between parallel stems. We believe the most significant conclusion of our analysis is that it predicts R_g to increase very slowly with M_w, in agreement with the data of Fig. 3. In fact R_g increases roughly as $\sqrt{\nu}$ (see Eq. (5) and Table 1) and in turn ν goes like $M_w/n_{stem} \sim (M_w)^{1/2}$, see Eq. (3), so that in conclusion we have

$$R_g \approx M_w^{1/4} \tag{6}$$

a result that is basically consistent with Fig. 3.

It should be pointed out that Eq. (6) cannot hold at very high degrees of chain collapse. In fact, in the limit of a single crystalline domain comprising the whole chain, density considerations dictate $R_g \approx M_w^{1/2}$.

4. The polymer chain in a bad solvent

It was already proposed by us [30–33] as well as by other Authors, most notably Muthukumar [36–38], that polymer crystallization is preceded by aggregation of chain segments into small pre-crystallization nuclei. In a sufficiently dilute solution these entities were regarded by us as intramolecular and denoted as bundles, see Fig. 7 [30–33]. The bundle state of the chain is to be regarded as meta-stable, its free energy being intermediate between the highest-energy free-chain state in solution and the lowest-energy crystalline state ($T < T_0$). Crystal formation proceeds from deposition of bundles onto a growing lamellar surface, see Fig. 7c. If the molecular length is below some limit, the probability of bundle formation is very small, as the chain is unable to create enough attractive interactions – both with itself and with the crystalline surface – to overcome the free-energy barrier contrasting fold formation. Under these circumstances the chain is rejected, i.e., segregated from the crystallization front [1–9,27–31]. It was shown that along these considerations a quasi-quantitative agreement between experimental evidence and statistical-mechanical predictions of chain segregation can be reached [31].

The statistical properties of the PE chain in the bundle state were described by one of us through a perturbative Grand Partition Function approach, assuming that any bundle represents a minor structural modification from the ideal solution state. The average chain fold length was evaluated starting from two different assumptions, namely Model A and Model B [31], later adopted again with relatively minor changes to achieve mathematical simplification [32,33]. Here it will be sufficient to stress that Model A-bundles comprise a three-stem core with shorter surrounding stems, see Fig. 7b. Conversely, in Model B-bundles, in addition to

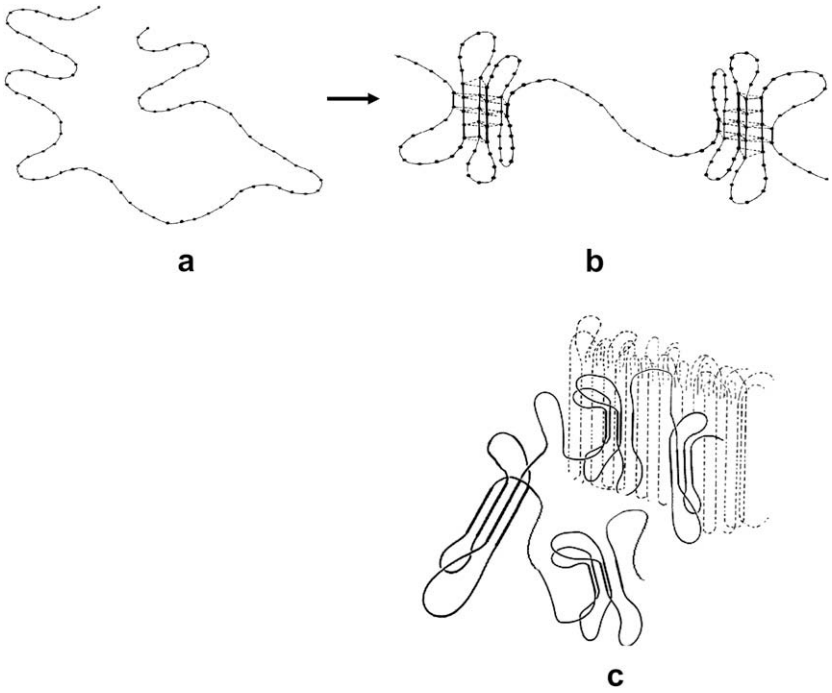

Fig. 7. (a) Schematic representation of a "free" chain; (b) a chain with bundles; (c) a chain with a few bundles, collapsing in the vicinity of a lamellar surface. Chain atoms are roughly shown by dots, dashed lines in (b) stand for van der Waals' attractions between stems. Dashed vertical lines in (c) represent chain stems on the sidewall of a crystalline lamella.

the three-stem restriction, there are additional restrictions on the stem lengths, that may be roughly summarized as leading to a uniform stem length [32]. More complex bundle models, comprising more than one package of parallel stems interconnected by chain folds, proved to be hardly relevant from a statistical viewpoint and are disregarded here [32]. Considering that the original paper was published on a Journal currently dealing with non-polymeric subjects, and that some aspects of the matrix algebra were originally omitted [31], we report the statistical approach here again in Appendix B.

Fig. 8 shows the results of the average stem lengths $\langle N_c \rangle$ (number of C atoms per stem) and of stems per bundle $\langle n_{stems} \rangle$, for both Models at different temperatures $\leq T_0$. We see that both quantities stay finite at all temperatures. On the contrary, in the limit $T \to T_0^-$ the average length of the bridges between the bundles $\langle n_{br} \rangle$ goes to infinity [see Eq. (17B)] because the positive free energy contribution μ goes to zero, see Eq. (4B). In the same temperature limit the (average) lamellar thickness also goes to infinity because the lengths of the bundle folds and of the inter-bundle bridges tend to average out through a reeling-in mechanism. The bridges are eventually absorbed inside the bundles producing an average crystalline structure. Comparison with the experimentally observed initial fold length of the lamellar crystals is satisfactory [33].

We point out that the bundled chain is in a bad solvent, therefore tending to a collapsed state; the solvent would become ideal at the ideal temperature $T \to T_0 \approx 113\,^{\circ}C$, much larger than those at which the diffraction experiments were carried out (60–70 °C). The bundles are reciprocally repelled by the expanded, structurally irregular chain folds, which prevent them from fusing together. We believe the chain statistical results reported in Appendix B – originally evaluated ignoring bundle–bundle repulsion – are not significantly affected by the bad solvent effect, as the corresponding repulsive, solvent-mediated forces are relatively mild.

5. The molecular mechanism of crystallization

In the meta-stable bundle state the chain undergoes local statistical fluctuations, with a dynamic interchange of chain segments between the bundles and the inter-bundle bridges. On account of the collapse [48–52] the chain cannot overlap in space with other chains and is essentially confined within a volume, its shape depending on the contacting solid surfaces. The chain may crystallize if it comes in contact with suitable irregularities on a solid surface, possibly holes or expansions, acting as crystallization nuclei (see two crystallizing chains approaching the side surface of a growing lamella in Fig. 9a). Each nucleus gives birth to a chain crystalline domain; the average dependence of the number ν of such domains from the chain molecular weight M_w [empirically given by Eq. (3)] may be rationalised as follows.

We assume the chain crystalline domains, as seen orthogonal to the stems, may be regarded as fragments of a virtual circle with radius R; the molecular weight M is proportional to the circle area, so that $M \propto R^2$. The circumference length $C = 2\pi R$ may be regarded as the overall length of contact between the crystallizing chain and the growing lamella. The number ν of the domains, equal to the number of nuclei, is taken to be proportional to C, and we have

$$\nu \propto C \propto M^{1/2}; \quad n_{stem} \propto M/\nu \propto M^{1/2}, \tag{7}$$

where the same dependence is expected for $\nu_{average}$ and $(n_{stem})_{average}$ if we substitute the average M_w for M. We point out that we also have the same dependence of $n_{stem} = (n_{stem})_{average}$ vs. M_w through our analysis of WANS/SANS results see Eqs. (1)–(1′) in Section 2.

An interesting issue correlated wit Eq. (7) is: what is the chain average molecular weight (M_w) that produces a single crystalline domain/chain ($\nu = 1$) and what is its size (n_{stem})? Taking the corresponding quantities ($M_w = 29.000$, $n_{stem} = 11$, $\nu = 2.35$) from Table 1 and Fig. 2, we have from Eqs. (7) $M_w = 5.250$, $n_{stem} = 4.7$, $\nu = 1.0$ as an admissible combination. We notice that the resulting figure of n_{stem} (average number of stems per crystalline domain) is close to the figure theoretically evaluated at 60–70 °C for $\langle n_{stem} \rangle$ (average number of stems per bundle) with realistic parameters, see Fig. 8. It is tempting to conclude that the smallest crystalline domains derive from crystallization of single bundles, and that shorter chains will be unable to crystallize (chain segregation) [1].

During deposition of the crystalline domain of one chain onto the growing lamella (see Fig. 8a, dashed-line contour), a second chain may initiate its own deposition in a contiguous region (Fig. 9a, continuous-line contour). Crystalline domains from different chains may be incorporated in the same lamella at different times. As it may be seen in Fig. 9b, assuming that the lamellar edge remains basically straight at different times, crystalline domains from different chains may be incorporated into the lamella, with no predictable regularity. The coordinate of the lamellar edge along its normal axis is proportional to the crystallization time, assuming constant rate of crystallization.

The average resulting shape of the crystalline domains is elongated parallel to the (110) crystallographic directions, in agreement with morphological evidence, in particular lamellar decoration results suggesting a significant probability for adjacent chain folds along this direction [25]. Crystal-packing forces should be

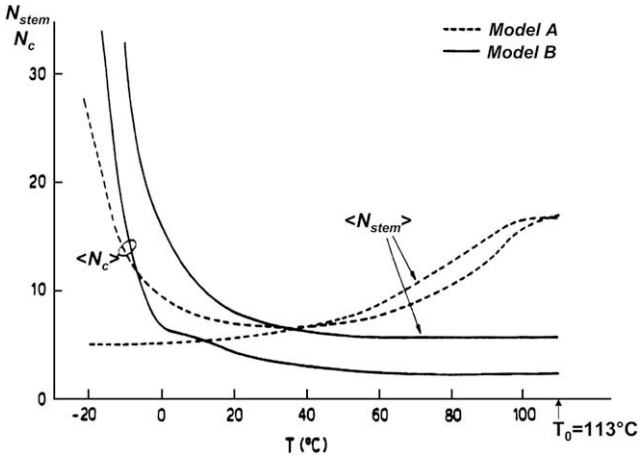

Fig. 8. Average number of stems per bundle ($\langle n_{stem} \rangle$) and of C atoms per stem ($\langle N_C \rangle$) at different temperatures, for Models A and B (see Appendix B, Eqs. (18B) and (19B), $\eta = 0.36$ kcal/mol; η is the attractive van der Waals' energy per C···C interaction within a bundle, see Appendix B.) (Figure derived from Fig. 4, Ref. [31]).

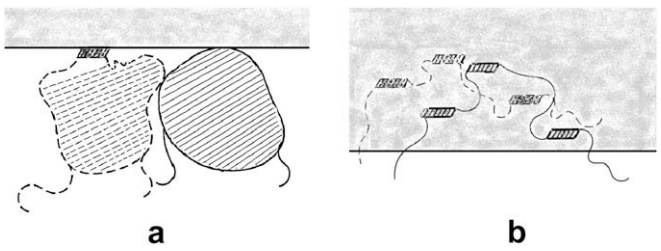

Fig. 9. a) At time t: Two chains projected on the lamellar plane. The dashed-line chain forms first and generates a crystalline domain after interaction with the lamellar surface. b) At time $t' > t$: From two chains we have two sets of crystalline domains, their orientation being along (110).

responsible for this as well as other structural aspects; in particular we point out that this elongation increases the number of favourable van der Waals' interactions between the stems of the domain under formation and those of the pre-formed lamella.

6. Discussion

6.1. From bundles to chain crystalline domains

According to the bundle theory [30–33], chain molecules in solution – to some, very limited extent in the molten state as well [33] – give rise to intramolecular associations, or "bundles", see Fig. 7. They may be regarded as "nematic precursors" of the polymer crystals, according to Muthukumar [38,48].

At temperatures of about 60° or 70 °C the "bundled" PE chains are well below the limiting dissolution temperature T_0 in *o*-xylene ($\approx$113 °C [54]). Consequently, each chain experiences a strong tendency towards collapse, which may be hindered by an insufficiently large molecular weight at a given temperature [49–52]. Steric repulsion between the individual bundles, mainly due to the relatively loose and irregular chain folds, hinders full collapse to a compact structure, as the chain still retains a substantial amount of solvent. However, as hinted in Fig. 9a, the collapsed chain structure prevents any chain–chain overlap. In the vicinity of the growing lamella, crystallization is originated by interaction of chain segments with suitable lamellar irregularities, or nuclei, see Fig. 9a and b. Assuming a uniform probability of nucleation per unit length of the contacting lamellar edge, both the average number of the crystalline domains and their average molar mass are $\propto M_w^{1/2}$, see Eq. (7). These conclusions appear to be in essential agreement with the SANS–IANS Kratky plots from partially deuterated samples obtained by Spells and Sadler [7] and by Stamm et al. [9]. Indeed, denoting by n_{stem} the average number of stems per crystalline domain, both (i) the power-law dependence $n_{stem} \propto (1/q^2_{peak}) \propto M_w^{1/2}$ for $29.000 < M_w < 380.000$ (Fig. 4) and (ii) the proportionality between n_{stem} and the weighted peak intensity (Fig. 5), support the approximate proportionality of n_{stem} with $M_w^{1/2}$. This result appears to be further supported by comparison of the radius of gyration R_g observed by Sadler and Keller through SANS experiments [4–6], with a bead-and-spring model of the crystallized chains predicting $R_g \propto M_w^{1/2}$ see Fig. 6 and Table 1. As shown in Fig. 3, the experimental data are consistent with our model, taking a root-mean-square length of the connecting segments of about 80 Å. In Fig. 3 experimental data are also reported for melt-crystallized chains, suggesting in that case the unperturbed dependence $R_g \propto M_w^{1/2}$. From the general expression of the mean-square radius of gyration

$$R_g^2 = \frac{1}{6} C_\infty \langle N_{CH_2} \rangle l_{C-C}^2, \quad \langle N_{CH_2} \rangle \approx M_w/14, \quad l_{C-C} = 1.54\,\text{Å}, \qquad (8)$$

we derive the reasonably acceptable value of the characteristic ratio $C_\infty \cong 9$. Since polymer bulk crystallization is generally thought to produce only limited, local rearrangements of the crystallizing chains [33], the last result nicely confirms general consistency of the data reported.

A rather obvious question, not mentioned yet to this point, is: since there is no compelling reason to have an identical structure for all the crystalline domains produced by the chains in a sample with a given M_w, what is their statistical distribution? Although structural investigation of this issue is beyond the limits of this study, in Fig. 10 we show as an example the effect of the domain-shape variation on the diffraction profile, under the constraint that the total number of stems is invariant. Apart from the largest peak, additional diffraction bumps or holes appear to be smoothened by the averaging effect. Analogous results were obtained by us for the samples with $M_w = 29.000$ and 189.000, see Fig. 2.

6.2. The superfolding model [7,35]

Spells and Sadler [7] and Sonntag et al. [35] carried out a detailed diffraction profile analysis on the basis of a Markov-type statistical model of the stem-sheets distribution along the (110) crystallographic direction, allowing for correlation between adjacent sheets, i.e., superfolding. We point out that their approach cannot be extended as such to our statistical model. In fact, with our model the crystalline domains are essentially compact, with no voids inside. As a result we have a qualitative discontinuity with any low-order Markov-type description based on a linear statistical distribution of stems along (110) sheets, although ingenuously modified to account for sheet–sheet correlation, or superfolding [35]. In principle, an appropriate statistical distribution should also be considered within our model; in fact, not all the compact domains must be identical, see the example reported in Fig. 10. However, because of the compactness it would be easy to show that any Markov-type statistical description would require a large number of probability parameters.

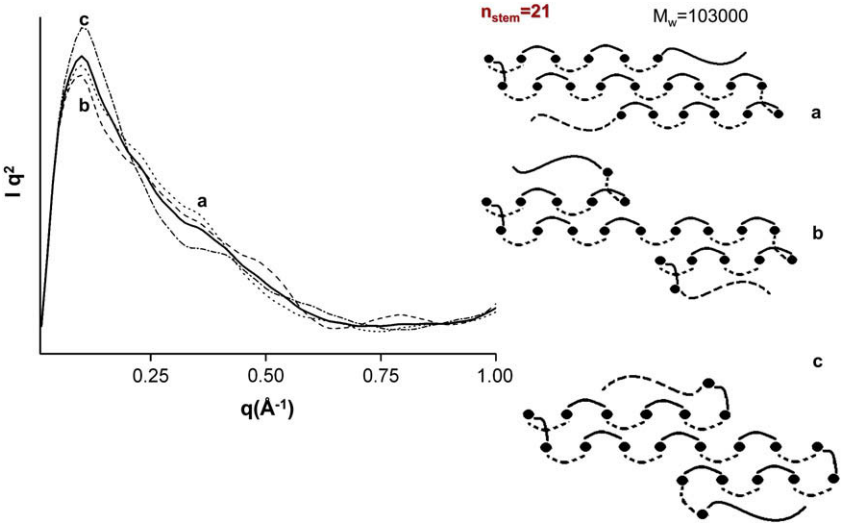

Fig. 10. Kratky plots from three different domain structures with the same number of stems n_{stem}. The average plot (continuous line) is smoother than the separate plots.

As an additional remark – with another difference from the model considered by the British Authors [7,35] – the compactness of the crystalline domains makes it impossible to have any dilution among them. However we may assume that some dilution is possible, so that a few stems not belonging to a tagged chain are present inside the domains shown in Figs. 1 and 2. We remark that the good correlation between the peak intensities shown in Fig. 5 dictates that the degree of dilution should be about the same for the 4 samples shown. More generally, the dilution assumption is in contrast with the molecular mechanism here proposed. In the assumption of many chains/domain, even the present satisfactory interpretation of the observed radius of gyration (see Figs. 3 and 6) would be made inconsistent by the requirement that all the crystalline domains should be connected by a complex framework of interconnecting chains.

6.3. The degree of adjacent chain folding

From the schemes reported in Figs. 1 and 2, showing the stem distribution in space, we evaluate an average probability $P_A = 0.85$ for a stem to be followed by another stem within the same crystalline domain. Identifying P_A with the probability of adjacent chain folding along the crystallographic direction (110), our result appears to be larger than the figure $P_A = 0.75$ suggested by Spells and Sadler [7] and by Sonntag et al. [35] on the basis of both neutron scattering and IR [23] results. However, if more irregular stem arrangements also contributing to the statistics were taken into consideration (see Fig. 10, e.g.,), the estimated figure of P_A would decrease towards 0.8 or less. As a conclusion, we believe the previously estimated figure $P_A = 0.75$ is not inconsistent with our statistical description.

6.4. Orientation effects on the diffraction profiles

In the quoted paper [7], Spells and Sadler suggest that their diffraction results (see Fig. 2) should be corrected for orientation effects, as the lamellar mats in their samples are closely orthogonal to – i.e., the chain stems closely parallel to – the diffraction beam. Such a preferential orientation may cause systematic deviations of the observed scattering intensity at low q-values, compared with the isotropically oriented sample that is assumed in our diffraction calculations. Since all the peak intensities reported in Fig. 2 correspond to very low q-values, this remark should apply to all their 4 samples [7]. Accepting this remark as a significant warning, we point out that: the q-coordinate of Spells–Sadler peak intensities as well as their peak shapes appear to be consistent with those of the Stamm–Fischer–Dettenmaier–Convert sample, which are free of preferred orientation [9]. For this reason, and also considering the relatively large error bars affecting the q-peak coordinate (see Figs. 4 and 5), we carried out the present analysis on the assumption that the orientation effects inherent with Spells–Sadler's samples could be regarded as essentially random errors.

6.5. Other models of polymer crystallization

In the following we shall analyze concisely a few significant aspects of relevant model approaches to polymer lamellar crystallization.

Based on both experimental results and on computer simulation, the analysis carried out by Muthukumar is very detailed, encompassing several kinetic aspects [37,38,48]; one important aim is to provide verification of the Lauritzen–Hoffman theory [2,3]. Some of his ideas and conclusions concerning lamellar formation appear to be consistent with some of our viewpoints (see in particular the "baby nuclei", "smectic pearls" and "nematic precursors" [38]). The Author points out that, during the growth stage of the lamellar crystal, there are a variety of competing metastable states, and analyzes the subtle mechanisms by which they are frustrated by the conformational energy barriers [48].

Hu and Frenkel [29] investigated several aspects of polymer crystallization using a simple lattice model, through lattice statistics, Monte Carlo simulations and phase diagrams. The Authors suggest that single-chain crystallization is easiest if the polymer undergoes a previous coil-to-globule transition, and the temperature is not so low that the globule has reached a glass-like state.

Among several investigations on the subject [42–44], Yamamoto carried out a realistic computer modelling of 3D crystallization from the melt [46]. Investigation of the crystallization process of a single polymer chain in a vacuum on the crystalline substrate was carried out. Modelling of chain crystallization from the melt unexpectedly produced tapered lamellae, with a thickening growth along the chain axis accompanying the usual growth perpendicular to it.

Common aspects of the above discussed models, including our own, are: i) lamellar chain crystallization develops through a variety of non-equilibrium states and is a non-equilibrium state by itself, ii) some sort of driving force towards chain collapse is at the base of the whole process.

Strobl [18] proposed an interesting, general model of polymer crystallization, see Fig. 11. It is based on the assumption that a precursor mesomorphic layer solidifies into a "granular" layer, eventually producing the lamellar crystal. Apart from the different origin – Strobl's model derives from observation of the hexatic phase in n-alkanes [23] – we see formal analogies with the model proposed in this paper, after translating our chain superbundle into Strobl's mesomorphic layer and our crystalline domains into Strobl's granules. In spite of these analogies, we wish to stress that one basic aspect of our model is that each crystalline domain belongs to a single chain.

7. Concluding remarks

We stress three general remarks from the present study on solution crystallization of PE chains.

First, the present model can interpret rather satisfactorily the observed difference between the radius of gyration of melt- and solution-crystallized chains, see Fig. 3 and Table 1. In particular, the solution-crystallized chains – the object of the present investigation – appear to be remarkably collapsed with respect to the melt-crystallized chains, essentially unperturbed as far as the radius of gyration is concerned. In turn, this reflects the collapse of the bundled chain before crystallization, see Fig. 9.

Second, each chain crystallizes under the form of compact crystalline fragments. With reference to Fig. 9a, after formation of the bundled, collapsed chain, solvent still swells the chain. Upon crystallization we have solvent expulsion and formation of

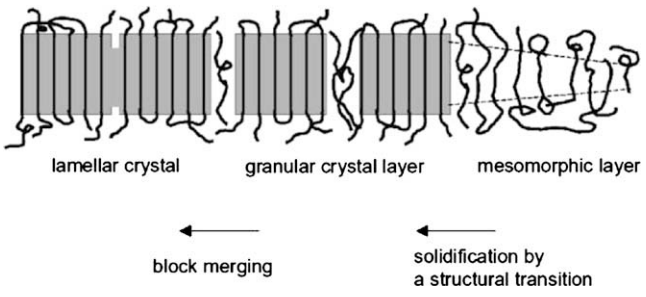

Fig. 11. The polymer crystallization model proposed by Strobl [18].

crystalline fragments, or domains, each of them originating from a secondary nucleus, see Fig. 9b. Assuming the probability of formation of the secondary nuclei along the lamellar edge to be independent of the molecular weight, the average number of crystalline stems within each domain (n_{stem}) turns out to be proportional to the square root of the molecular weight [see Eq. (7)], in basic agreement with observation. The overall number of crystalline domains is between 2 and 9 for M_w between 30.000 and 400.000, see Table 1. The experimentally observed radius of gyration R_g, see Fig. 3, is reasonably well explained by a statistical model whereby the crystalline domains and their connecting chain segments are uncorrelated in space (see Fig. 6 and Table 1). We point out that the intramolecular compact structure of the crystalline domains is also strictly correlated with the collapsed state of the chain before crystallization. Compact, collapsed chains cannot overlap in space; as a consequence they produce non-overlapping domains upon crystallization.

The third remark, from extrapolation of the data reported in Figs. 1 and 2, is that the smallest observable crystalline fragments – comprising about 5 parallel stems for polymer samples with $M_w \approx 5.000$ – are rather close in size to the single bundles in the pre-crystalline chain (about 8.5 or 5.5 stems for Models A and B respectively, see Fig. 8). As a reasonable conclusion, we suggest that i) the smallest crystalline domains derive from single bundles and that ii) chains much shorter than about 5.000 Da (about 350 C atoms) cannot crystallize according to the presently discussed mechanism (chain segregation).

Acknowledgement

The Authors thank Prof. Valdo S. Meille for very useful comments and suggestions as well as for very interesting discussions. They also acknowledge useful comments by Professor Manfred Stamm.

Appendix A. Calculation of the scattered intensity

We deal with the intensity scattered by a random mixture of deuterated/hydrogenated PE chains. The algorithm used by us to evaluate the Kratky plots by sets of parallel polymer stems is very simplified. We checked it to be adequate in the reciprocal coordinate range under investigation [$0 < q(=4\pi \sin\theta/\lambda) \leq 0.25$ Å^{-1}] comparing the results with more precise calculations. The scattering centres are identified with pseudo-atoms repeating after a constant distance of 1.27 Å along straight lines coinciding with the stem axes, 100 scattering centres being placed on each stem; the scattering by atoms belonging to chain folds is neglected. The parallel stem axes are disposed according to a hexagonal setting – a rough approximation to the monoclinic, pseudo-hexagonal structure of PE – and the scattering centres have the same axial coordinates in all the stems. Defining an integer i going from 1 to the total number $n_s \cdot 100$ of scattering centres, we have ($q < 1$) [9]

$$q^2 \cdot I(q) = C \cdot (b_H - b_D)^2 \sum_{i=1}^{n_s \cdot 100} \sum_{j=1}^{n_s \cdot 100} \frac{4\pi q \sin(q \cdot d_{ij})}{d_{ij}};$$
$$d_{ij}^2 = \Delta_{ij}^2 + (z_j - z_i)^2;\ q = \frac{2\pi \sin\theta}{\lambda} \quad (1A)$$

where b_H, b_D respectively are the scattering lengths of hydrogen and deuterium, d_{ij} is the distance between C atoms, 2θ is the diffraction angle and λ the wavelength. The i-th C atom coordinate along the stem axis is z_i and Δ_{ij} is the distance between the stem axes where the atoms i and j belong. For all the stems we have the same set of z_i coordinates. The sum in Eq. (1A) is extended to all the stems of the crystalline domain, see Figs. 2 and 10 for examples.

Appendix B. The statistical properties of the crystallizing chain

In the following we summarize the statistical–mechanical equilibrium approach first proposed in Ref. [31] and utilized further by some of us [32,33].

We assume the polymer system to consist of a single, extremely long chain with N (>1) identical chain atoms, in a bad solvent. At the limiting dissolution temperature T_0 the chain is regarded as unperturbed, long-range interactions being absent. At this temperature the partition function of a N-bond chain ($N > 1$) may be written as

$$Z_{N0} = Z_N(T = T_0) = \sum \Omega_N \exp\left(-\frac{E_N}{k_B T_0}\right) = \lambda^N, \quad (1B)$$

[Ω_N, E_N] respectively being the multiplicity factor and the energy of the generic conformational state of the chain. We shall assume that, for each conformation, the energy E_N is defined with respect to the energy of the chain in solution at $T = T_0$.

At $T < T_0$, $(T_0 - T) < T_0$, the chain is able to partly crystallize; its partition function $Z_N(T)$ increases above λ^N, due to the negative-energy terms correlated with crystallization. We assume that the chain undergoes a pre-crystallization state – that we identify with the bundle state – before full-fledged, lamellar crystallization is achieved. In the bundle state the relative amount of monomer units involved in crystal-like (i.e., attractive) van der Waals' interactions is small, which makes it convenient to express $Z_N(T)$ in a perturbative form:

$$Z_N(T) = Z_{N0} + \sum_b \Omega_b [\exp(-E_b/k_B T) - \exp(-E_b/k_B T_0)]. \quad (2B)$$

the sum being carried out over the bundle configurations of the chain. Here we stress that any bundle-like chain configuration at the crystallization temperature T (see Fig. 7) is already counted in the partition function Z_{N0}, except for the different temperature [i.e., $T < T_0$ for $Z_N(T)$, $T = T_0$ for Z_{N0}]. Although the present approach was initially devised for a chain with bundles interconnected with randomly oriented, unperturbed bridges [31], we believe it may be extended with a reasonable approximation to the superbundle model, wherein each bundle is in van der Waals contact with its neighbours, still retaining its identity.

We follow the Grand Partition Function approach, specifically adopting Model A utilized by one of us in Ref. [31]; the $[-CH_2-]_N$ chain will be schematically modelled as a sequence of identical atoms with an average bond angle of 180°, see Fig. [7] as an example. In view of Eqs. (1B) and (2B) may be written as

$$\Xi(T) = \sum_{N=1}^{\infty} \frac{Z_N(T)}{\lambda^N} \exp(-N\mu)$$
$$= \sum_{N=1}^{\infty} \left\{ z^N + \sum_b \frac{\Omega_b z^b}{\lambda^b} [\exp(-E_b/k_B T) - \exp(-E_b/k_B T_0)] \right\};$$
$$z = \exp(-\mu), \quad (3B)$$

where $\Xi(T)$ is the GPF of the chain ensemble, $-k_B T \mu$ ($\mu > 0$) is the free energy per bond, μ a chemical potential and b is the number of bonds comprised in the generic chain bundle, see Fig. 7b. [In Eq. (3B) the term z^N in curly brackets stand for the completely free-chain state ($E_b = 0$).] As shown in the figure, the chain configuration is always viewed as an alternation of bridges (i.e., free-bonds

sequences) and bundles; bundle associations involving distant chain atoms will be disregarded in view of their negligible probability.

Let us consider first the free-bond sequences, i.e., the bridges between bundles, see Fig. 7b. Labelling with n the number of chain atoms comprised therein, and with $n(\min)$ their minimum value their grand statistical weight is

$$\zeta(\mu) = \sum_{n=n(\min)}^{\infty} z^n = \frac{z^{n(\min)}}{1-z} = \frac{\exp[-\mu\cdot n(\min)]}{1-\exp(-\mu)} \cong \frac{\exp[-\mu\cdot n(\min)]}{\mu}, \quad (4B)$$

where the assumption is made that the undercooling degree $(T_0-T)/T_0$ is sufficiently small compared with unity that $(0<)\ \mu<1$.

The bundle structure will be regarded as statistically emanating from a central core consisting of 3 stems of identical length ($\overline{n}$ chain atoms), see Fig. 7. Specifically, an additional stem may be added to the central core provided that

i) it produces hexagonal packing with two core stems,
ii) it is connected fold-wise to one of these core stems,
iii) it is as long as, or shorter than, the core stems, i.e., it comprises $n \le \overline{n}$ chain atoms.

The process will be repeated in an endless fashion, i.e., each time a stem is added to the bundle provided it is no longer than either stem it packs with. As a result, following the chain contour the stem lengths n_i will obey the rule:

$$n_1 \le n_2 \le n_3 \le \ldots \le n_{k-1} = n_k = n_{k+1}[=\overline{n}] \ge n_{k+1} \ge n_{k+2} \ge \ldots n_p \quad (5B)$$

We see that, except for the terminals, each stem is connected by a chain fold to two stems in the same bundle; no stem may be longer than the core stems ($\overline{n}$ chain atoms).

Before evaluating the Grand Partition Function (see Eq. (3B)), we turn now to the bundle structure (see again Fig. 7), evaluating separately the GPF contributions of:

a) the chain folds; b) the bundle core consisting of 3 identical stems; c) the extra-core stems.

We proceed in a sequence:

a) The Grand Partition Factor of the folds is given by

$$\varphi(\mu) = \sum_{n=m(\min)}^{\infty} P(n,\Delta v)\cdot\exp(-\mu\cdot n), \quad (6B)$$

where $P(n,\Delta v)$ is the probability of closure – within a small volume Δv – of a "ring" comprising n chain bonds. In the freely jointed chain approximation $P(m,\Delta v)\propto \Delta v/(l\cdot m)^{3/2}$ and we have

$$\varphi(\mu) = Q\cdot\sum_{m=m(\min)}^{\infty}\exp(-\mu\cdot m)m^{-3/2}, \quad (7B)$$

where Q is a pure number proportional to $\Delta v/l^3$ (we take $Q=1$). With linear PE, at current temperatures the minimum number of chain bonds for ring closure is roughly $m(\min)\approx 15$–20 [31].

b) The bundle core consists of three stems with identical length, each comprising a variable number $\overline{n}$ of chain atoms $(1 \le \overline{n} < \infty)$. We assume that the chain continuity is maintained within the core, so that two chain folds are required, one at each opposite end, as shown in Fig. 7b. The corresponding Grand Partition Factor is

$$K(\overline{n},T,\mu) = \left[\exp(-3\mu\cdot\overline{n}+3\eta\cdot\overline{n}/k_BT)/\lambda^{3\overline{n}}\right]\varphi^2(\mu)/2, \quad (8B)$$

where η is the packing energy per $(CH_2)\cdots(CH_2)$ contact. It is convenient to construct a diagonal matrix $\mathbf{K}(T,\mu)$ summarizing this result for different values of $\overline{n}$:

$$\mathbf{K}(T,\mu) = \begin{bmatrix} K(1,T,\mu) & 0 & 0 & 0 & \ldots \\ 0 & K(2,T,\mu) & 0 & 0 & \ldots \\ 0 & 0 & K(3,T,\mu) & 0 & \ldots \\ 0 & 0 & 0 & K(4,T,\mu) & \ldots \\ \ldots & \ldots & \ldots & \ldots & \ldots \end{bmatrix}, \quad (9B)$$

where a convenient upper limit for $\overline{n}$ is around 20.

c) Denoting the length (i.e., number of chain atoms) of any non-core stem with the symbol n, considering that each atom feels two packing interactions with previously placed stems of the bundle, the GPF of the stem is

$$H(n,T,\mu) = \left[\exp(-\mu\cdot n+2\eta\cdot n/k_BT)/\lambda^n\right]\varphi(\mu). \quad (10B)$$

It is convenient to construct a square matrix $\mathbf{H}$ where the row index is given by n (i.e., the atom length of the stem) whereas the column index equals the atom length of the previously placed stem: with reference to (5B), if $p(<k-1)$ is the number index of the stem being considered, the number index n_1 of the previously placed stem is $p+1$. Supposing that the length of the $(p+1)$th stem is n', the (n,n') element of $\mathbf{H}$ is given by

$$H(n,n') = (n'-n+1)\left[\exp(-\mu\cdot n+2\eta\cdot n/k_BT)/\lambda^n\right]\varphi(\mu) \quad (11B)$$

The multiplicity factor $(n'-n+1)$ is equal to the number of ways of placing a shorter stem (length: n chain atoms) over a longer stem (n' chain atoms). The structure of the resulting matrix is:

$$\mathbf{H} = \begin{bmatrix} H(1,1) & 2H(1,1) & 3H(1,1) & 4H(1,1) & \ldots \\ 0 & H(2,2) & 2H(2,2) & 3H(2,2) & \ldots \\ 0 & 0 & H(3,3) & 2H(3,3) & \ldots \\ 0 & 0 & 0 & H(4,4) & \ldots \\ \ldots & \ldots & \ldots & \ldots & \ldots \end{bmatrix} \quad 12B$$

(The zero-elements reflect the prohibition of placing any stem adjacent to a shorter stem.) We are able now to evaluate the Grand Partition Factor of the bundles $\Theta(T,\mu)$. We have

$$\theta(T,\mu) = \Theta(T,\mu) - \Theta(T_0,\mu) \quad (13B)$$

where

$$\Theta(T,\mu) = [1\ 1\ 1\ 1\ldots]\ \mathbf{H}(T,\mu)\cdot\mathbf{K}(T,\mu)\cdot\tilde{\mathbf{H}}(T,\mu)\begin{bmatrix}1\\1\\1\\1\\\ldots\end{bmatrix}, \quad (14B)$$

where pre- and post-multiplication by unit line and column vectors stands for the sum over bundles with all possible stem lengths.

Evaluation of averages from the Grand Partition Function

As shown in Fig. 7b, the polymer chain is represented by a sequence of independent parts, namely the bridges and the bundles. Consequently, denoting with ζ and Θ the corresponding Grand Partition Factors (GPF), we may write for $\Xi(T)$, see Eqs. (3B) and (13B):

$$\Xi(T) = \zeta\cdot\theta + (\zeta\cdot\theta)^2 + (\zeta\cdot\theta)^3 + \ldots = \frac{\zeta\cdot\theta}{1-\zeta\cdot\theta}. \tag{15B}$$

(We remark that the right-hand side is a function of the chemical potential μ, in addition to the temperature T.) It is convenient to introduce the fixed-point constraint of infinite chain length, that leads to

$$1 - \zeta\cdot\theta = 0; \quad \theta(T,\mu)\cdot\zeta(\mu) = 1, \tag{16B}$$

where ζ and θ are defined in Eqs. (4B) and (13B). From (4B) the average chain atom length of the bridges between bundles is

$$\langle n_{\mathrm{br}}\rangle = -\frac{\partial \ln \zeta}{\partial \mu} = n(\min) + \frac{\exp(-\mu)}{1-\exp(-\mu)} = n(\min) + \frac{z}{1-z}, \tag{17B}$$

where $n(\min)$ is negligible with respect to the second term for small undercooling degrees, i.e., $\mu \to 0$. Analogously, from Eq. (13B) we have the average number of chain atoms in the bundles:

$$\langle n_{\mathrm{bun}}\rangle = -\frac{\partial \ln \theta(T,\mu)}{\partial \mu} \tag{18B}$$

whereas the average number of stems per bundle is

$$\langle N_{\mathrm{stem}}\rangle = \frac{\partial \ln \theta(T,\mu)}{\partial \ln \varphi(\mu)} + 1, \tag{19B}$$

where $\varphi(\mu)$ is the GP Factor of a stem-connecting fold, see Eq. (7B). Similarly, all the relevant bundle averages may be evaluated.

We point out that with the present formalism we have described a statistical model (denoted by us as Model A) where the bundle probability is approximated by excess because the fold probability is regarded as constant no matter whether the atoms directly connected in neighbouring stems are at the same height or not (see Fig. 7b). Another model, denoted as Model B, was also considered by us [31], which suffers from the opposite limitation. Namely, the terminal C atoms of the stems connected by a fold are constrained to stay in contact; as a consequence, all the numerical factors larger than unity in the matrix **H** (see Eq. (12B)) are reduced to 1. It is possible to show that Model B may be approximated in turn by keeping all the bundle stems of identical length [32,33].

References

[1] Wunderlich B. Macromolecular physics, vols. 1 and 2. New York: Academic Press; 1976.
[2] Lauritzen Jr JI, Hoffman JD. J Appl Phys 1973;44:4340.
[3] Hoffman JD, Thomas Davis G, Lauritzen Jr JI. In: Hannay NB, editor. Treatise on solid state chemistry, vol. 3. New York: Plenum Press; 1976.
[4] Sadler DM, Keller A. Macromolecules 1977;10:1128.
[5] Sadler DM, Keller A. Science 1979;203:263.
[6] Sadler DM. In: Hall I, editor. The structure of crystalline polymers. London: Elsevier; 1983. p. 125.
[7] Spells SJ, Sadler DM. Polymer 1984;25:739.
[8] Wignall GD. Physical properties of polymers. 2nd ed. Washington, DC: ACS Professional Reference Book; 1993. p. 313–78 [chapter 7].
[9] Stamm M, Fischer EW, Dettenmaier M, Convert P. Faraday Discuss Chem Soc 1979;68:263.
[10] Strobl G. The physics of polymers. Berlin Heidelberg, New York: Springer; 1995.
[11] Nakatani AI, Dadmun MD, editors. Flow-induced structure in polymers, ACS symp ser 597. American Chemical Society; 1995.
[12] Geil PH. In: Fakirov S, editor. Handbook of thermoplastic polyesters. Weinheim: Wiley; 2002. p. 105.
[13] Al-Hussein M, Strobl G. Eur Phys J E 2001;6:305.
[14] Grasruck M, Strobl G. Macromolecules 2003;36:86.
[15] Bassett DC, Block S, Piermarini GJ. J Appl Phys 1974;45:414.
[16] Bassett DC. In: Bassett DC, editor. Developments in crystalline polymers. London: Appl Sci Publ; 1982. p. 115 [chapter 1].
[17] Ungar G. Polymer 1993;34:2050.
[18] Strobl G. Eur Phys J E 2000;3:165.
[19] Rastogi S, Ungar G. Macromolecules 1992;25:1445.
[20] Guinier A. Ann Phys Paris 1939;12:161.
[21] Wang H. J Polym Sci 2004;42:3133.
[22] Cho TY, Stille W, Strobl G. Macromolecules 2007;40:2596.
[23] Strobl G, Cho TY. Eur Phys J E 2007;55:23.
[24] Cheam TC, Krimm S. J Polym Sci Polym Phys Edn 1980;19:423.
[25] Wittmann JC, Lotz B. J Mater Sci 1986;21:659–68.
[26] Lotz B. Eur Phys J E 2000;3:185.
[27] Flory PJ. Statistical mechanics of chain molecules. New York: Interscience; 1969 [chapter 7].
[28] Yamamoto T, Miyaji H, Asai K. Jpn J Appl Phys 1977;16:1891.
[29] Hu W, Frenkel D. Adv Polym Sci 2005;191:1.
[30] Allegra G. J Chem Phys 1977;66:5453.
[31] Allegra G. Ferroelectrics 1980;30:195.
[32] Allegra G, Meille SV. Phys Chem Chem Phys 1999;1:5179.
[33] Allegra G, Meille SV. Adv Polym Sci 2005;191:87.
[34] Armistead K, Goldbeck-Wood G. Adv Polym Sci 1992;100:219.
[35] Sonntag P, Care CM, Spells SJ, Halliday I. J Chem Soc Faraday Trans 1995;91:2593.
[36] Liu C, Muthukumar M. J Chem Phys 1998;109:2536.
[37] Muthukumar M. Adv Chem Phys 2004;128:1.
[38] Muthukumar M. Adv Polym Sci 2005:191.
[39] Yoon DY, Flory PJ. Polymer 1977;18:509.
[40] Imai M, Kaji K, Kanaya T. Macromolecules 1994;27:7103.
[41] Kaji K, Nishida K, Kanaya T, Matsuba G, Konishi T, Imai M. Adv Polym Sci 2005;191:187.
[42] Yamamoto T. J Chem Phys 1997;107:2653.
[43] Yamamoto T. J Chem Phys 1988;89:2356.
[44] Yamamoto T. J Chem Phys 2001;115:8675.
[45] Yamamoto T. J Macromol Sci 2003;B42:629.
[46] Yamamoto T. Adv Polym Sci 2005;191:37.
[47] Meyer H, Müller-Plathe F. Macromolecules 2002;35:1241.
[48] Muthukumar M. Lecture Notes Phys 2007;14:1.
[49] Allegra G, Ganazzoli F. Macromolecules 1983;16:1311.
[50] Allegra G, Ganazzoli F. J Chem Phys 1985;83:397.
[51] Ganazzoli F, Raos G, Allegra G. Macromol Theory Simul 1999;8:65.
[52] Ganazzoli F, Kuznetsov YA, Timoshenko EG. Macromol Theory Simul 2001;10:325.
[53] Allegra G, Ganazzoli F, Bignotti F, Bolognesi M. Biopolymers 1990;29:1823.
[54] Miller RL. Kolloid-Zeitschrift & Zeitschrift für Polymere 1968;225:68.

Professor Giuseppe Allegra. Professor of Chemistry at the Department for Chemistry, Materials and Industrial Chemistry at the Polytechnic of Milan. Graduated in Chemical Engineering at the Politecnico di Milano under the guidance of Giulio Natta, Nobel Prize for Chemistry 1963, he started his academic career as a close associate of Giulio Natta and Paolo Corradini. He was visiting professor of Chemistry at the Polytechnic Institute of Brooklyn in 1969. Full professor at the Trieste University from 1970 to 1973, professor of Chemistry at the Polytechnic of Milan thereafter. First president of the Italian Association for Macromolecules (AIM, in 1975), from 1979 to '81 he was president of the Italian Crystallography Association (AIC) and later president of the Commission of Crystallography of the National Research Council (CNR) for three years. Director of the "Ettore Maiorana" International School on Direct Methods in Crystallography at Erice (Sicily) in 1978, and director of the Workshop on "Polymer Conformation and Dynamics" in Galzignano, 1985; this Workshop was attended by de Gennes, Edwards, Stockmayer. From 1993 to 1998 he was the first president of the Macromolecular Consortium among Italian Universities (CISM), and titular member of the IUPAC Subcommittee on Macromolecular Terminology for about 20 years to the present. From 1975 to '81 he was a co-editor of Acta Crystallographics for 6 years and member of the Editorial Boards of several International Journals. Since 2003 he is a member of the Accademia Nazionale dei Lincei. – His scientific interests range from crystallography of organometallics and polymers, to polymer statistical mechanics and polymer crystallization.

Dr. Antonino Famulari. He graduated in Chemistry with merit at the University of Milan. In 1998, he completed his Ph.D. course in the field of molecular modelling. He had several research grants by the Consiglio Nazionale delle Ricerche and a contract of research (1999) in the field of chemistry at the Dipartimento di Chimica Fisica ed Elettrochimica, Università degli Studi di Milano. In 2000 he was appointed at a permanent research position by the CNR center ISTM of Milan. Since December of 2001 he is assistant professor at the Dipartimento di Chimica, Materiali e Ingegneria Chimica of the Politecnico di Milano in the research group of Professor Giuseppe Allegra. At the beginnings of his research activity, he worked on the development of methods for the calculation of accurate intermolecular interactions; the approaches are available as standard options in general software such as GAMESS-US and MOLPRO packages. He collaborated with several international research groups (Professor M. S. Gordon, Iowa State University; Professor D. L. Cooper, University of Liverpool). Currently he is working on: (i) molecular modeling (from molecular mechanics and dynamics to ab initio approaches) and (ii) X-ray scattering methodologies (WAXD and SAXS techniques). Main research interests: structure and morphology of polymers, oligomers, polymer/clay composites and nano-composites; intermolecular interactions characterization including ionic liquids and systems of biological interests. He is the co-author of more then 60 scientific papers on various international journals.